Understanding connected surface-water/groundwater systems using Fourier analysis of daily and sub-daily head fluctuations

Acworth, R. I.; Rau, Gabriel C.; McCallum, Andrew M.; Andersen, Martin S.; Cuthbert, Mark O.

DOI:
10.1007/s10040-014-1182-5

Understanding connected surface-water/groundwater systems using Fourier analysis of daily and sub-daily head fluctuations.

Journal:	*Hydrogeology Journal*
Manuscript ID:	HJ-2014-3122.R2
Category:	Paper
Date Submitted by the Author:	n/a
Complete List of Authors:	Acworth, Richard; UNSW Australia, Connected Waters Initiative Research Centre Rau, Gabriel; UNSW Australia, Connected Waters Initiative Research Centre McCallum, Andrew; UNSW Australia, Connected Waters Initiative Research Centre Andersen, Martin; UNSW Australia, Connected Waters Initiative Research Centre Cuthbert, Mark; UNSW Australia, Connected Waters Initiative Research Centre; University of Birmingham, School of Geography, Earth and Environmental Sciences
Keywords:	Australia, analytical solutions, confining units, groundwater/surface-water relations, groundwater hydraulics

Understanding connected surface-water/groundwater systems using Fourier analysis of daily and sub-daily head fluctuations

R. I. Acworth[1], Gabriel C. Rau[1], Andrew M. McCallum[2], Martin S. Andersen[1], Mark O. Cuthbert[1,3]

1. Connected Waters Initiative Research Centre (CWI), School of Civil and Environmental Engineering, UNSW Australia, King Street, MANLY VALE 2093, Australia.

2. Affiliated with Connected Waters Initiative Research Centre, UNSW Australia.

3. School of Geography, Earth and Environmental Sciences, University of Birmingham, Edgbaston, B15 2TT, UK

Email: i.acworth@unsw.edu.au;

Tel: +61 2 80719826

Fax: +61 2 99494188

Abstract

The long-term monitoring records of hydraulic heads frequently contain fluctuations originating from different cyclic drivers. Fourier analysis applied to these records can reveal connected surface-water/groundwater system characteristics. The various components of the atmospheric tides, the earth tides and the presence of diurnal responses to evapotranspiration are identified and isolated through band-pass filtering of data recorded from both vented and absolute gauge transducers. The signature of the different cyclic drivers is contained in amplitude and phase of the various signal components and can be used to determine the degree of system confinement. A methodology is described for the calculation of barometric efficiency in confined aquifers based upon the amplitude of the M_2 and S_2 components of the earth and atmospheric tides. It is demonstrated that Fourier analysis of water-level fluctuations is a simple but underused tool that can help to characterise shallow groundwater systems.

Keywords: Australia, Analytical solutions, Confining units, Groundwater/surface-water relations, Groundwater hydraulics

1. Introduction

Signal analysis techniques are routinely used in many areas of the earth sciences (Davis, 1973) with sophisticated packages in use in the geophysics industry or the area of coastal engineering (Doodson, 1921; Emery & Thompson, 2004). Despite early work in the groundwater field by Weeks (1979), van der Kamp and Gale (1983), Hsieh et al, (1987), Rojstaczer (1988a, 1988b), Rojstaczer and Agnew (1989), Rojstaczer and Riley (1990), for example, and the regular use of signal analysis techniques in other disciplines, there is little evidence of their routine use in hydrogeological studies. This is unfortunate as this early work demonstrated that signal analysis could be used to derive a much improved understanding of the impacts of mechanical loading of confined aquifers and to the determination of barometric efficiency and specific storage. Where signal analysis techniques have been used in hydrogeology (for example Weeks (1979), Hsieh et al, (1987) or Merritt (2004)), the analysis has been for either deep confined or deep unconfined aquifer systems. Work in shallow connected surface water groundwater systems has concentrated on the diurnal variation in water level that could be related to evapotranspiration effects (Gribovszki et al 2010; Johnson et al, 2013).

The measurement of water levels for hydrogeological investigations is often considered a trivial task but needs to be undertaken carefully if the full range of important information contained in the data set is to be sensibly extracted (Post & von Asmuth, 2013). Where absolute gauge measurements (transducer diaphragm sealed on the reference side to a vacuum or a fixed pressure) are made with a transducer suspended at a fixed depth in the bore/piezometer, the logger records the total pressure on the transducer diaphragm. This includes the pressure of the water column above the point of measurement and the pressure of the overlying air. In simple terms, if the overlying air pressure can be measured by another logger separately, it can be separated from the pressure exerted by the height of the water column and removed by subtraction. This is the recommended approach of many manufacturers of absolute pressure gauge transducers sold into the groundwater market. The accuracy of the derived water pressure measurement is therefore directly related to the accuracy of the atmospheric pressure measurement and simultaneous measurements are essential. It is the necessity to accurately measure the atmospheric pressure variation that has prompted our revised interest in the causes of the daily and sub-daily head fluctuations caused by atmospheric pressure variation and what we can learn about the aquifer system by observing this response.

Price (2009) has demonstrated that the data derived from the correct use of absolute gauge transducers are the same as that obtained for vented gauge transducers, as long as the system accuracy is sufficient. A vented gauge transducer makes the correction for atmospheric pressure automatically by subjecting the opposite side of the transducer diaphragm to atmospheric pressure via the use of a thin pipe extending from the transducer to the atmosphere (Price, 2009). Sorensen and Butcher (2010, 2011) give an extensive review of the accuracy of available logging systems.

In this paper we use signal analysis techniques based on the Discrete Fourier Transform (DFT) on a long sequence (35,000 data points with 96 measurements per day) of groundwater data from a connected surface water - groundwater environment at Maules Creek in Northern New South Wales, Australia. Results are presented from a stream gauge (vented transducer), loggers in two unconfined piezometers and a logger in a confined piezometer (absolute gauge transducers). We describe applications of Fourier signal analysis techniques to both vented and absolute gauge data and demonstrate how the use of this approach can assist with hydrogeological interpretation of long data series from a shallow groundwater environment connected to a stream. In particular, we show how the use of a DFT pair, where the time series data is shown alongside the frequency spectrum, can also be used to detect Earth tides (indicating a confined aquifer response) and calculate the barometric efficiency of an aquifer, or to detect the presence of evapotranspiration in a riparian zone.

2. Methodology

2.1. Catchment Description

A site on Maules Creek in Northern New South Wales, Australia (Latitude: -30.5°, Longitude: 150.08°, Elevation 253 m Australian Height Datum (AHD)), is used to demonstrate the use of the DFT pair in this study. The site has been described in previous papers (Andersen and Acworth, 2009; Rau et al., 2010; McCallum et al, 2013) and only background data will be repeated here.

Figure 1

Maules Creek is a tributary to the Namoi River that drains into the Darling River and is a part of the Murray-Darling River Basin. The creek is largely ephemeral, but has a perennial section in its middle reach at Elfin Crossing (Fig. 1) that is fed by groundwater discharge from a shallow coarse grained aquifer. At low-flow conditions, the surface-water flow in Maules Creek at this middle reach is exclusively controlled by surface-water/groundwater interactions (Andersen and Acworth, 2009), since the reaches above and below dry out except when the creek is in flood. There is a permanent flow gauge at Elfin Crossing that was established by the NSW Government with real-time data available on the web (Waterinfo, 2013). The water level at this gauging station is recorded using a vented transducer with a cable running from the pool and buried in the bank up to the gauging station hut. Details and pictures can be seen on the web site. Low flow discharge from this gauge is reported to be below approximately 10 ML/day (115 L/s).

A climate station is installed at a site at Bellevue Farm, some 11 km due west from Elfin Crossing where temperature, incoming solar radiation, wind and rainfall are measured amongst other parameters (Fig. 1).

Shallow piezometers were installed in a wooded area to the east of the creek (e.g. EC 17 on Fig. 2) using a Geoprobe pneumatic hammer to drive casing through the coarse alluvium. This method met refusal at a few metres depth. A large rotary rig equipped with a 300 mm combination percussion air-hammer and casing advance system (TUBEX) was used to achieve greater penetration on the west bank and boreholes BH 7 and BH 12

(Fig. 2) were completed, each with multiple piezometers installed isolated by a cement seal. Drill records (BH 12) indicate a sequence of sandy gravels with some clay to a depth of approximately 17 m. A clay layer is present between 25 and 30 m depth which has a significant impact on hydraulic heads with a consistent reduction in head (i.e. downward gradient) of approximately 1.25 m. Details of the piezometers and boreholes for which water level records are presented are given in Table 1.

The banks of the creek are lined with mature River Red Gums (*Eucalyptus camaldulensis*) that often have their trunks standing in surface water. The lower part of the catchment between Elfin Crossing and the junction with the Namoi River is extensively flood irrigated using a combination of groundwater abstraction from deeper parts of the alluvial aquifer and Namoi River water (Andersen and Acworth, 2009). Except under flood conditions, surface flow in Maules Creek ceases at some point between Elfin Crossing and the Namoi River as a result of losses to the underlying aquifer. The location of this cease to flow point can rapidly move upstream as a response to the start of groundwater abstraction and flow conditions at Elfin Crossing appear to be permanently impacted with significant downward gradients beneath the pool at Elfin Crossing (Rau et al., 2010) as noted above. The alluvial material that forms the base to the river channel has been cut into Permian coal measures (Maules Creek Formation) that are under active exploration by mining companies.

Figure 2

Table 1

2.2. Water level measurement

In this paper we use water levels that were recorded with a combination of vented and unvented (absolute pressure) loggers. Absolute gauge transducers (Solinst Levelogger Gold and Edge) were used at EC 17, BH 12.2 and BH 7.1 Atmospheric pressure was measured using a Solinst Barologger installed at 2 m below ground level and above the water level in BH 8 (Fig. 2). We recorded water levels with a time resolution of 96 cycles per day (cpd) corresponding to 15 minute time intervals so that linkages between the surface stream (flood response) and the groundwater system could be accurately resolved.

2.3. The Discrete Fourier Transform (DFT)

The DFT of a long set of regularly spaced data, such as that provided by data logging of a groundwater level at a regular time interval, can be expressed in the frequency domain as a sequence of individual sinusoids (Fourier, 1822) that collectively add to make up the original signal. The mathematical expression of the DFT is as follows (e.g. Smith, 2007):

$$X(k) = \sum_{n=0}^{N-1} x(n)\, e^{-i2\pi\frac{kn}{N}}, \qquad \text{Equation 1}$$

where: $X(k)$ is the frequency spectrum corresponding to the time series $x(n)$,. In other words, Eqn. 1 transfers data from the time domain (where it is a series of measurements of a given parameter made at a constant time interval) to the frequency domain (where it can be represented by a plot of frequencies against the amplitude of that frequency). The Inverse Discrete Fourier Transform (IDFT), where data can be transferred from the frequency domain to the time domain, is defined as (e.g. Smith, 2007):

$$x(n) = \frac{1}{N}\sum_{k=0}^{N-1} X(k)\, e^{-i2\pi\frac{kn}{N}}. \qquad \text{Equation 2}$$

For a detailed discussion of the DFT and its mathematical properties the reader is referred to Oppenheim and Schafer (1999), Emery & Thomson (2004) or Smith (2007). The graphical representation of data in both the time domain and the frequency domain can be referred to as a DFT pair (see Fig. 3 for an example).

It is noteworthy that the resolution in the frequency domain is directly linked to the resolution in the time domain, i.e. the sampling frequency of water levels. The mapping of higher frequencies is therefore limited by the sampling rate in the time domain, as the correct identification of any particular sinusoidal component requires at least 2 samples within one period. The latter is referred to as the Nyquist frequency (f_N) expressed as:

$$f_N = \frac{1}{2\Delta t} = \frac{f_s}{2},$$ Equation 3

where: Δt is the sampling time interval, or f_s is the sampling frequency. It is important to acknowledge that any energy from signal components with frequencies higher than that will be contained (aliased) in the spectrum but cannot be identified separately.

The selection of a water level sampling frequency is therefore an important consideration and forms a compromise between the requirements for measuring rapid water level variations and available resources for data transmission, storage and manipulations.

2.4. Fourier analysis and filtering

The DFT (Eqns. 1-2) is a fundamental component of many signal processing software packages. It is commonly implemented as an algorithm called the Fast Fourier Transform (FFT) and Inverse Fast Fourier Transform (IFFT) which efficiently solve the DFT (Eqn. 1) and IDFT (Eqn. 2) numerically. Examples for popular software packages particularly suited to signal processing are Matlab, Mathematica (commercial), R, Octave and PyLab (open source).

In this paper we work with the software package TSoft (Van Camp and Vauterin, 2005). TSoft is free software available for the Windows operating systems (TSoft, 2013). The package allows the application of a variety of filters, including those based on the Fourier Transform, and provides excellent graphical applications for data display. The results of data logging can be saved as a text file and imported into TSoft using the free format specifier (TSoft, 2103). It is assumed that the data is regularly sampled in time and the user is prompted for a start date and time and the sample interval (s) upon data import. For more details refer to the TSoft manual available online.

An example of Fourier analysis using the DFT on water levels is illustrated in Fig. 3 where 3 typical frequencies found in groundwater monitoring, viz, a signal repeating at 2 cycles per day (12 hour period), 1 cycle per day (24 hour period) and at 0.2 cycles per day (5 day period) can be added together to show a sequence often seen in atmospheric pressure data. Here, the 5 day variation represents the somewhat variable mesoscale pressure variation typical for the movement of low pressure systems. This example also illustrates the linearity of the DFT whereby no information is lost in the transform calculation between the time domain and the frequency domain. An excellent example of the use of signal processing is given by Hsieh et al (1987).

Figure 3

The frequency domain is particularly useful for data manipulation, as it allows the extraction of a signal with a certain frequency that can be unclear in the time domain data. This process is referred to as filtering. Undesired frequencies can be removed by applying a weighting function to the data in the frequency domain. Three common filters are available; low pass, high pass and band-pass functions. The first two only allow the lower and the higher frequencies beyond a desired ‘cut-off’ value to pass when the signal is transformed back into the time domain. The latter removes both lower and higher frequencies and requires an additional bandwidth parameter defining the width of the frequency window (on either side of the cut-off). Acworth and Brain (2008) illustrated the use of these filters in their study of groundwater levels in shallow granites. In this paper, we apply a band-pass FFT implemented in TSoft in order to investigate the phase and amplitude of various frequencies at 1cpd or greater representing atmospheric tides, Earth tides or other processes. The FFT uses a windowing technique to allow the variation in amplitude of a specific frequency throughout the complete signal. One side effect of the bandpass filtering is the edge effect introduced at the beginning and the end of the filtered time series.

3. RESULTS AND INTERPRETATION

3.1. Atmospheric Pressure

A DFT pair of atmospheric data for a 9 month period sampled every 15 minutes (96 cpd) is shown in Fig. 4.

Figure 4

The complete frequency spectrum of the recorded atmospheric pressure is shown with data up to 48 cpd (the Nyquist frequency for logging at 96 cpd), although there is very little energy for frequencies greater than 3 cpd (8 hourly). The amplitude and frequency plot clearly show the higher amplitude energies associated with mesoscale pressure variations at frequencies of less than 0.5 cpd. However, very clear and separate peaks also occur at 1 and 2 cpd (In following figures the spectrum is truncated at 3.5 cpd and amplified for clarity).

The peaks at 1 cpd (denoted S_1) and 2 cpd (denoted S_2) in atmospheric pressure data were recognised shortly after the invention of the barometer by Torricelli in 1643 (Ananthakrishnan et al, 1984). There has been much debate about their origin. They are not gravitational tides as they do not vary with lunar time (Thomson (Lord Kelvin), 1882). It is considered that they are associated with thermal energy caused by heating the upper atmosphere as the earth rotates (Palumbo, 1998). The primary generating signal is approximately a square wave, corresponding to the sun rising and then setting 12 hours later as the earth rotates. The amplitude and phase of this S_1 wave were extracted from the signal (Fig. 4) using a FFT based band-pass filter with a cut off at 1.0 cpd and a band width of 0.05 cpd. The maximum occurs at 12:00 and the minimum at 00:00. However, the amplitude of this wave varies considerably throughout the seasons (Acworth and Brain, 2008). By contrast, the 2 cpd wave (FFT band-pass filter with cut off at 2.0 cpd and a bandwidth of 0.05 cpd) has maxima at 04:00 and 16:00 with corresponding minima at 10:00 and 22:00 and has almost constant amplitude with time.

Thermo-tidal theory (Chapman and Lindzen, 1970) is used to explain the tides with solar heating and the inclusion of energy dissipation in the atmosphere due to ozone and water vapour excitation being the main casual agents. In general, the S_2 is predicted by this theory to have larger amplitude and is much more regular than S_1. This is explained by the S_1 tide being produced by a regionally varying number of interfering wave components that are mutually destructive. It is seen that the theory accounts for most of the observations but can still not account for the fact that the observed maximum in S_1 occurs at 10:00 local time instead of the theoretically predicted 09:00 local time.

There are various processes that can influence the observed water level signal in a well at 1 cpd or 2 cpd. For this reason, we will refer here to the S_1 and S_2 atmospheric tides as S_{1a} and S_{2a} in the analysis that follows. Irrespective of the processes responsible for the formation of S_{1a} and S_{2a} we can still use this very regular excitation of the ground and the response of the groundwater level, to determine barometric efficiency (Jacob, 1940). The regularity of the S_{1a} and S_{2a} components is a significant advantage over using the much more variable mesoscale response at frequencies below 0.5cpd and we will return to this later.

3.2. Surface Water Levels at Elfin Crossing Stream Gauge

Figure 5

There is a permanent deep pool between the line of the bores and the surface water transducer installation. Since a vented gauge transducer was used at this site, there is no evidence of any atmospheric pressure signal in the record (Figure 5).

There is a small amplitude signal at 1 cpd in the amplitude and frequency plot of the creek data (Figure 5). This is can be resolved using a FFT band-pass filter (cut off at 2.0 cpd with a bandwidth of 0.02 cpd) to be a frequency with a maximum at 08:00 in the morning and a minimum at 20:00 in the evening. This should not be confused with a barometric pressure response (S_{1a}) that has a maximum at 12:00 and a minimum at 00:00. The amplitude of the water level response is also much smaller than the S_{1a} of the atmospheric data (Fig 5). Note also the lack of resolution in the output from the transducer deployed at the site as the time series data for the hydraulic head shows step changes.

3.3. Borehole Records

The data from BH 7.1 (Fig. 6), EC 17 (Fig. 7) on the opposite bank under the trees, and BH 12.2 (Fig. 8) on the north-west bank of the area are presented. These loggers were each of the absolute pressure type (Details in Table 2). To facilitate comparison, each of the 3 figures shows DFT pairs of three components: the atmospheric pressure at BH 8; the uncorrected output for the data logger showing the total pressure head (atmospheric and water); and the hydraulic head (total pressure head with the atmospheric component removed by subtraction and referenced to Australian Height Datum (AHD)).

3.3.1. Borehole 7.1

Figure 6

Borehole 7 contains piezometers at 248 m AHD (BH 7.1) and 242 m AHD (BH 7.2) installed in a mixture of sands and gravels that are hydraulically connected to the Creek, as seen from their response to floods. The middle plot in Fig. 6 shows the total pressure head (water plus atmosphere) recorded by the absolute gauge pressure transducer. It is clear that the total pressure head is strongly influenced by the atmospheric pressure (top panel in Fig. 6) and in phase with the atmospheric pressure. The strong 1 and 2 cpd spectra (S_{1a} and S_{2a} components) are clearly seen in the amplitude and frequency plot shown to the right of the time series data. Note that the time series data is only a subset of the complete record, selected to best represent the variability in the data set and at the same time visualise the variability at the important frequencies. The Fourier analysis to derive the amplitude and frequency plot was carried out on the complete record of data, but in the plot, the record is shown only to 3.5 cpd as there is no significant energy contained in the frequency spectrum between 3 cpd and the Nyquist frequency (48 cpd).

The lower plot in Fig 6 shows the hydraulic head record with the atmospheric signal removed (by subtraction). The strong variability noted in the middle plot (time series) is completely removed while the amplitude frequency plot shows a simple distribution with a slight frequency component at 1 cpd, but no energy at 2 cpd. The S_{1a} and S_{2a} signals have been eliminated.

In theory the water pressure at the water table represents atmospheric pressure (Domenico and Schwartz, 1998; Ingebritsen et al, 2006). Accepting this definition, removal of the atmospheric component from the total pressure head in a perfectly unconfined aquifer should leave only the elevation head of the water table. An aquifer should be considered perfectly unconfined if air can move down through the formation instantaneously in response to changes in atmospheric pressure. Norum and Luthin

(1988) investigated the conditions generated by an advancing wetting front and demonstrated that confined conditions could be generated for a time if the air in the unsaturated zone was unable to escape.

As the thickness of the unconfined zone increases; resistance to air flow, the hydraulic conductivity of the material and the radius of the well can all influence the well response (Rojstaczer and Riley, 1990) producing the possibility that unconfined aquifers can show a response to atmospheric pressure change, albeit with a significant phase lag and diminished amplitude. However, the shallow well depths in this study (<30 m), the small diameter of the piezometers (50 mm) and the relatively high hydraulic conductivity of the sands and gravels all make this unlikely. The absence of any response to atmospheric pressure in the data presented (Fig 6) confirm this analysis.

Examination of the phase of the remaining 1 cpd energy using TSoft shows a maximum at 05:00 and a minimum at 17:00 and is not to be confused with the atmospheric energy at the same frequency (S_{1a}) of much greater amplitude and a different phase.

3.3.2. Piezometer EC 17

In contrast to the data from BH 7.1, EC 17 is located in trees on the opposite bank of the creek. The screened depth is approximately 6 m below ground surface with the elevation of the screen set at 4 m below the water table. The corrected hydraulic head response of this piezometer (Fig. 7) is similar to that of BH 7.1 (Fig 6) and the creek (Fig 5), confirming that this piezometer is in an unconfined portion of the aquifer system. As with the other two water table responses, there is a strong observed signal at 1 cpd that has a maximum at 06:00 and a minimum at 18:00. There is an interesting phase lag of the 1 cpd signal between BH 7.1 at 248 m AHD and EC17 at 250m AHD, of approximately 1 hour that requires further investigation.

Figure 7

3.3.3. Borehole 12.2

BH 12 was completed close to BH 7 (Figs 1 and 2) to provide a vertical profile of piezometers on the west side of the creek. BH 12.2 was completed at approximately 229 m AHD and lies beneath a confining layer of clay. It is not clear from the available drilling data how laterally extensive this clay layer is. The hydraulic head at BH 12.2 is approximately 1.25 m below that at BH 7.1, indicating a significant downward gradient.

The total pressure head is dominated by the atmospheric pressure (Fig. 8), similar to BH 7.1 and EC 17. There is also a small response at a frequency of approximately 1.9 cpd visible in the total head data (middle plot in Fig. 8). Importantly, subtraction of the atmospheric pressure leaves a residual impact where the response is now inverted (lower plot in Fig. 8) and as predicted for confined aquifers by Jacob (1940). This is clearly seen in the time series data (Fig. 9) where a reduction in atmospheric pressure is matched by an increase in hydraulic head. BH 7.1 is included in Fig.9 to demonstrate the difference in response between the unconfined BH 7.1 and BH 12.2.

Examination of the DFT pair for the corrected data (Fig. 8 lower plot) shows five small peaks that have the same frequencies as the earth tides (Bredehoeft, 1967) shown in Table 2 (Wahr, 1995; Merritt, 2004). Note also that the small response in the total pressure plot (middle plot in Fig. 8) is now recognised as the M_2 lunar frequency at 1.93 cpd.

Figure 8

Figure 9

Table 2

FFT band-pass filters were used to investigate the characteristics of the 1.0, 1.93 and 2.0 cpd signals of the BH 12.2 record in the time domain with the results shown in Fig. 10. The 1.0 cpd component has a distinct seasonality in amplitude with maxima corresponding to the solar solstices at mid-June and mid-December with a minimum in mid-September at the equinox. This response is believed to be the result of superposition of both earth tides (K_1) and atmospheric tides (S_{1a}), noting again that S_{1a} is expected to vary seasonally. The 1.93 cpd component shows very constant amplitude throughout the record and is seasonally independent. This component is the main lunar semi-diurnal (M_2) signal emanating solely from the Earth tide response. The 2.0 cpd component shows some seasonality but less than the 1.0 cpd component and is not clearly associated with the seasons. The observed signal is believed to be the result of superposition of the S_{2a} (atmospheric tide) and S_2 (earth tide) components. The variations seen at the beginning and end of each record may be attributed to edge effects caused by the band-pass filter.

Figure 10

The various amplitude changes (Fig. 10) for the different frequency components of the hydraulic head in BH 12.2 reveal a complex situation. The observed 1.0 cpd and the observed 2.0 cpd signals in the BH 12.2 spectrum are the result of several processes. Atmospheric pressure and earth tides are both incorporated. However, the 1.93 (M_2) signal appears to only be caused by the Earth tide at this frequency. The amplitude and suggested causes of the various tide components identified by the DFT in the data are given in Table 3, with data for BH 7.1 and EC 17 included for comparison.

Table 3

4. DISCUSSION

4.1. Optimising the sampling frequency of water levels

Inspection of the atmospheric data in Fig. 4, or any of the DFT pairs (Figs 5 to 8) indicates that there is no significant information at a frequency of greater than 3 cpd. Using the Nyquist frequency, it is clear that sampling at 6 cpd will satisfactorily resolve a periodic signal at 3 cpd. Following this logic, sampling every 4 hours (6 cpd) will recover all the components of the groundwater signal. Sampling at greater than 6 cpd could therefore be considered as oversampling and wasteful of system resources. However, we acknowledge that the timing of non-sinusoidal events like the arrival of a flood peak could require a higher sampling frequency depending on the desired resolution of the shape of the flood hydrograph.

4.2. Evapotranspiration and its spectral signature

A significant 1.0 cpd signal exists in piezometers installed in the unsaturated zone (Maules Creek surface water level shown in Fig. 5, BH 7.1 in Fig 6 and EC 17 shown in Fig. 7). This is not an earth tide response as the other earth tide components are absent and is also not a residual of an atmospheric pressure response as there is no S_{2a} component. The probable explanation for this response is photosynthetic demand by phreatophytes (groundwater extracting plants) on the aquifer system during daylight hours (e.g. White, 1932; Loheide et al., 2005).

To prove this hypothesis, solar radiation is plotted together with water levels for the BH 9 (Fig. 2) record in Fig. 11. Although the solar radiation data is from a site 11 km distant, there will not be significant variation from the Elfin Crossing site. Daily short-wave radiation totals (MJm^{-2}), potential evaporation and rainfall (mm) are also shown in Fig. 11. The concordance between solar radiation and potential evaporation is entirely expected. The observation that water levels fall as soon as the solar radiation begins at the start of the day and continues until the sun sets, after which water levels begin to recover complies with the literature (e.g. Butler et al., 2007; Gribovszki et al., 2010). These data show that the roots of the phreatophytes growing around the site, large river red gums, reach into the gravel aquifer at Elfin Crossing and act like cyclic groundwater pumps.

The period between 6th and 8th November was cloudy and there was little incoming short-wave radiation received. The lack of photosynthesis by the trees over this period is clearly shown by the absence of the daily drawdown in the groundwater level indicating that the 'groundwater pumps' had been closed down over this period.

Figure 11

Further detail on the photosynthetic activity can be provided by analysing the 1.0 cpd signal after isolating it using a FFT band-pass filter. The time series of 1.0 cpd signals for EC17, BH 7.1 and the creek are shown in Fig. 12.

Figure 12

The amplitude of the EC 17 site is considerably larger than that at BH 7.1 closer to the creek. There is also a phase lag (not shown) of between 15 min and 1 hr, with BH 7.1 leading EC 17. A very clear increase in amplitude in EC 17 and BH 7.1 is also seen as the solar radiation input increases between winter and summer.

The decrease of the fluctuation in amplitude towards the creek may be attributed to the increasing supply of surface water (Butler et al., 2007; Johnson et al., 2013) in combination with the spatial distribution of the phreatophytes (with less trees near BH 7.1). It is also interesting to note that the amplitude of the 1.0 cpd signal for the creek does not show the same degree of seasonality as that for EC 17 and BH 7.1.

Water level fluctuations induced by phreatophytes have extensively been exploited for the quantification of evapotranspiration (e.g. White, 1932; Loheide et al., 2005; Gribovszki et al., 2010) including the estimation of surface water and groundwater fractions consumed (Johnson et al., 2013). However, the spectral signature of these fluctuations and its usefulness for the determination of surface water groundwater connectivity has not yet been reported. Fig. 12 illustrates clearly the usefulness of the Fourier analysis approach.

4.3. Earth tide signals and the confined aquifer response

At the unconfined BH 7.1, air is able to move through the unsaturated zone above the water table so that the water table represents atmospheric pressure. Subtracting the atmospheric pressure signal from the total pressure, recorded by the absolute gauge transducer, completely removes the atmospheric components recorded in the total pressure record. This is clearly shown in Figs. 6 and 7 and is not surprising given the shallow depth to the water table (approx. depth 1 – 2 m), the small diameter of the piezometer tube (30 mm) and the relatively coarse grained nature of the sediments at Maules Creek. Each of these factors will act to supress the possibility of atmospheric tides in the unconfined aquifer (Rojstaczer and Riley, 1990).

However, when the atmospheric pressure is deducted from the total pressure signal for BH 12.2, a different result occurs in that the response to atmospheric pressure is not removed but (partially) inverted. This is shown in Figs. 8 and 9 and can be conceptualised as the result of removing too much of the pressure signal from the record thus causing the inversion. More erudite explanations are provided by Jacob (1940), van de Kamp & Gale (1983), Merritt (2004), Ingebritsen et al (2006) and Price (2009): The reason for the over-correction is that only a part of the atmospheric loading is initially transferred to the water column in a confined aquifer with the balance of the load supported by the aquifer skeleton. Subtracting all the atmospheric pressure therefore provides too much of a correction. It is noted that a vented transducer will produce the equivalent result with the same partial inversion of the atmospheric signal.

The amplitude and phase of the atmospheric pressure record at 1.0 cpd and 2.0 cpd and the hydraulic head data for the BH 12.2 record are shown in more detail in Fig.13. The amplitudes for these data have been kept the same in these plots so that the comparative size can be appreciated. There is significant seasonal variation shown in both the 1.0 cpd atmospheric data, and to a lesser extent in the 1.0 cpd data for BH 12.2 (Fig 13 a). Interestingly, there is a significant phase difference between the two data sets (Fig. 13 b) of approximately 5 hours. This is instead of the 12 hours that would be expected if the atmospheric tide loading was expressed in the hydraulic head record as a simple inversion. We take this to indicate that there is interference from an Earth tide component (K_1) at the same frequency as the atmospheric pressure component (S_{1a}), but of a different phase.

Figure 13

The 2.0 cpd signals for the atmospheric pressure and for the BH12.2 record show no seasonal variation (Fig 13 c). Furthermore, the phase lag between the individual components is closer (5.5 hours) to the expected 6 hours (Fig 13 d).

4.4. Estimate of barometric efficiency from the ratio of the S_2 and M_2 amplitudes

Jacob (1940) demonstrated that the barometric efficiency of an aquifer could be calculated from the ratio of the aquifer response to the atmospheric pressure change driving that response. It has been demonstrated above that the very clear atmospheric signal at 1 and 2 cpd produces an equally clear response in the hydraulic head data at the same frequencies. However, the 1 cpd data is significantly impacted by seasonal variation and other factors so that it would be beneficial to use the 2 cpd signal for this calculation. We have also noted that the 2 cpd signal in the hydraulic head comprises the input from both the atmospheric tide (S_{2a}) and the Earth S_2 tide. It is useful to define this (hydraulic head) response as S_{2h}, where

$$S_{2h} = S_{2h-a} + S_{2h-earth}. \qquad \text{Equation 4}$$

We can also define a hydraulic head response to the M_2 earth tide as M_{2h}. The barometric efficiency can be calculated from the ratio of S_{2a} and S_{2h-a}.

To derive a value for $S_{2h-a,}$ we need to find a value for $S_{2h-earth}$. Fortunately, we can use the theoretically calculated Earth tides with the measured value of M_{2h} to provide this value. The Tsoft package (Tsoft, 2013) can be used to calculate the theoretical value of the earth tides for a given latitude and time. The ratio of the amplitude of the M_2 and S_2 components of the Earth tide will be constant. We can use this ratio along with the value of M_{2h} to derive $S_{2h-earth}$.

In Fig. 14, the earth tides at 1.93 and 2.00 cpd (M_2 and S_2) are shown for Maules Creek (tide shown in red scaled on the left hand axis). The observed data for BH 12.2 over this frequency spectrum is also shown in Fig. 14 (tide shown in blue and scaled on the right-hand axis).

Figure 14

At Maules Creek, the ratio of the S_2:M_2 Earth tides is 0.488 (shown in Fig. 14). The M_{2h} (1.93 cpd) signal in the observed response can be multiplied by the ratio (0.488) to derive the earth tide component $S_{2h-earth}$. Subtraction of $S_{2h-earth}$ from S_{2h} allows recovery of the atmospheric component of the observed data (S_{2h-a} in Fig. 14) previously hidden in S_{2h}.

S_{2h-a} can then be used to calculate the barometric efficiency (BE) of the aquifer (Jacob, 1940; van de Kamp & Gale, 1983)

$$BE = \frac{dh}{dp} = \frac{S_{2h-a}}{S_{2a}} = \frac{0.000564}{0.00815} = 0.069 . \qquad \text{Equation 5}$$

The components in Equation 5 are given in terms of metres head, as the atmospheric pressure is recorded as a head (Table 3) rather than a pressure, by the logger software. The calculated value of BE is low (a rigid aquifer would have a BE of 1.0) and suggests that the aquifer material is not rigid but deformable. This is entirely consistent with our knowledge of the geology from the drilling records.

If we assume that undrained conditions apply at the frequencies involved (Rojstaczer, 1988) and recognise that (Jacob, 1940, van de Kamp and Gale, 1983)

$$BE = 1 - \gamma, \qquad \text{Equation 6}$$

where γ is the loading efficiency. Parameter γ can be expressed as a ratio of terms involving compressibility

$$\gamma = \frac{\alpha}{\theta\beta + \alpha}, \qquad \text{Equation 7}$$

where α is the material compressibility and β (= 4.4 x 10^{-10} Pa^{-1}) is the fluid compressibility (at a temperature of 20°C), and θ is the porosity. Equation 7 can be rearranged to provide solutions for α given an appropriate value for the porosity. For example α = 1.187 x 10^{-9} Pa^{-1} for a typical porosity of 0.2. Values of compressibility for undrained and unconsolidated media are not often measured as they are not of interest to the geotechnical industry however Berryman (2010) provides some values for undrained and unconsolidated sands that are of the same order.

With α, β and θ either known or assumed, the value of specific storage for the formation

$$S_s = \rho g(\alpha + \theta\beta) \qquad \text{Equation 8}$$

can also be calculated. This approach gives a value of 1.25x10^{-5} for the specific storage ($\theta = 0.2$). The use of the barometric efficiency to generate a value of specific storage is of great use in regional groundwater analysis (Harrington and Cook, 2011, and many others).

5. CONCLUSIONS

This paper illustrates how Fourier analysis of water level data using the Discrete Fourier Transform (DFT) provides a useful tool to examine water level data in the frequency domain. Significant frequencies in the data can be easily resolved, in contrast to the great difficulty in resolving these separate high frequency signatures in the time domain. More importantly, the amplitude and phase of these frequencies can be isolated and then plotted back in the time domain so that their relationship to physical processes can be better explored.

In this paper we have made use of data sets collected with both vented and non-vented (absolute gauge) transducers. Inspection of this data in the frequency domain reveals the presence of significant tides at a frequency equal to, or greater than, one cycle per day. These are generated by a mixture of thermally derived atmospheric tides, earth tides and changes caused by variation in evapotranspirative fluxes. The data for a variety of unconfined and confined head data is analysed.

Unconfined aquifer data shows that the thermally induced atmospheric tides are not retarded in their progression through the unsaturated zone and they are completely removed by subtraction of the atmospheric pressure from the total pressure measured by absolute gauge transducers installed at the site.

The recognition of the characteristic Earth tide frequencies (O_1, K_1, M_2, S_2 and N_2) in the frequency spectrum for a deeper piezometer at the site indicates that the aquifer is confined at this location. Under confined conditions, the response at the piezometer is formed by a mixture of thermal atmospheric tides and earth tide components. A method of separating these components is described and the barometric efficiency is determined.

Fourier analysis also helps to determine the best sampling frequency for long-term groundwater monitoring by considering the necessary resolution in both time and frequency domain. The analysis demonstrates that a sampling interval of 4 hours (6 cpd) is sufficient to capture the essential system characteristics illustrated in this study. It is recommended that data logging for long-term groundwater monitoring move towards the less frequent measurement unless there are other grounds for maintaining more frequent measurements.

Acknowledgements

Aspects of this paper were first presented in September 2012 at the IAH 49th Congress in Niagara Falls, Canada. The site at Elfin Crossing on Maules Creek has been established using funds provided by the Cotton Catchment Communities CRC as a part of their Catchment Research program. Funding for GCR was provided by the National Centre for Groundwater Research and Training, an Australian Government initiative, supported by the Australian Research Council and the National Water Commission. The NSW Office of Water maintains the Elfin Crossing Stream gauge. Borehole and logger installations were only possible by funding from The Australian Government Groundwater Educational Investment Fund (GEIF). MOC was supported by the European Community's Seventh Framework Programme [FP7/2007-2013] under grant agreement n°299091. The authors are grateful to Edwin Weeks and two other anomimous reviewers for their helpful comments.

References

Acworth RI, Brain T (2008) Calculation of barometric efficiency in shallow piezometers using water levels, atmospheric and earth tide data. Hydrogeol J 16:1469-1481. DOI 10.1007/s10040-008-0333-y

Ananthakrishnan R, Maliekal JA and Aralikatti SS (1984) Atmospheric tidal oscillations Part 1. Historical Development. Current Science 53.18:945-951.

Andersen MS, Acworth RI (2009) Stream-aquifer interactions in the Maules Creek catchment, Namoi Valley, New South Wales, Australia. Hydrogeol J 17:2005-2021

Berryman JG (2010) Inverse problem in anisotropic poroelasticity: Drained constants from undrained ultrasound measurements. Lawrence Berkeley National Laboratory http://escholarship.org/uc/item/5nb876j3.

Bredehoeft JD (1967) Response of well-aquifer systems to earth tides. J Geophys Res 72:3.075 – 3.087

Butler JJ, Kluitenberg GJ, Whittemore DO, Loheide SP, Jin W, Billinger MA, Zhan X (2007) A field investigation of phreatophyte-induced fluctuations in the water table. Wat Resour Res 43:W02404, doi:10.1029/2005WR004627.

Chapman S, Lindzen RS (1970) Atmospheric Tides – Thermal and Gravitational. Reidel, Dordrecht-Holland.

Davis JC (1986) Statistics and data analysis in Geology – Second Edition. John Wiley & Sons Inc., New York.

Doodson AT (1921) The harmonic development of the tide-generating potential. Proc Roy Soc London A100:305-329.

Domenico PA, Schwartz FW (1998) Physical and Chemical Hydrogeology, 2nd Ed, Wiley.

Emery WJ, Thomson RE (2004) Data analysis methods in physical oceanography (2nd Edition). Elsevier.

Fourier JBJ (1822) Analytical theory of heat, Didot.

Gribovszki Z, Szilágyi J, Kalicz P (2010) Diurnal fluctuations in shallow groundwater levels and streamflow rates and their interpretation – A review. J Hydrol 385:371-383.

Harrington G, Cook P (2011) Mechanical loading and unloading of confined aquifers: implications for the assessment of long-term trends in potentiometric levels. Waterlines Report Series No 51, National Water Commission, Australian Government.

Hseih PA, Bredehoeft JD, Farr JM (1987) Determination of Aquifer Transmissivity from Earth Tide Analysis. Water Resour Res 23.10:1824-1832.

Ingebritsen S, Sanford W, Neuzil C (2006) Groundwater in Geologic Processes 2nd Ed, Cambridge University Press.

Jacob CE (1940) On the flow of water in an elastic artesian aquifer. American Geophysical Union Transactions, Part 2, p 574-586.

Johnson B, Malama B, Barrash W, Flores AN (2013) Recognizing and modeling variable drawdown due to evapotranspiration in a semiarid riparian zone considering local differences in vegetation and distance from a river source. Wat Resour Res 49:030-1039. doi:10.1002/wrcr.20122.

Loheide SP, Butler JJ, Gorelick SM (2005) Estimation of groundwater consumption by phreatophytes using diurnal water table fluctuations: A saturated-unsaturated flow assessment. Water Resour Res 41:W07030. doi:10.1029/2005WR003942.

McCallum AM, Andersen MS, Giambastiani BMS, Kelly BFJ, Acworth RI (2013) River-aquifer interactions in a semi-arid environement stressed by groundwater abstraction. Hydrol Proc 27:1072-1085.

Merritt LM (2004) Estimating Hydraulic Properties of the Floridan Aquifer System by Analysis of Earth-Tide, Ocean-Tide, and Barometric Effects, Collier and Hendry Counties, Florida. USGS Water-Resources Investigations Report 03-4267.

New South Wales Department of Primary Industries, Office of Water website. http://waterinfo.nsw.gov.au/ (Accessed 15 January, 2014).

Norum DI, Nuthin JN (1968) The effects of entrapped air and barometric fluctuations on the drainage of porous mediums. Water Resour Res 4.2:417-424.

Oppenheim AV, Schafer RW, Buck JR (1999) Discrete-time signal processing. Prentice Hall, Upper Saddle River.

Palumbo A (1998) Atmospheric tides. J Atmos Sol-Terr Phys 60:279-287

Post VEA, von Asmuth JR (2013) Review: Hydraulic head measurements-new technologies, classic pitfalls. Hydrogeol J 21: 737-750.

Price M (2009) Barometric water-level fluctuations and their measurement using vented and non-vented pressure transducers. Q J Eng Geology Hydrogeol 42: 245-250. doi:10.1144/1470-9236/08-084.

Rau GC, Andersen MS, McCallum AM, Acworth RI (2010) Analytical methods that use natural heat as a tracer to quantify surface water-groundwater exchange, evaluated using field temperature records. Hydrogeol J 18:1093-1110.

Rojstaczer S (1988a) Determination of Fluid Flow Properties From the Response of Water Levels in Wells to Atmospheric Loading. Water Resour Res 24.11:1927-1938.

Rojstaczer S (1988b) Intermediate period response of water levels in wells to crustal strain: sensitivity and noise level. J Geophys Res 93.B11:619-634.

Rojstaczer S, Agnew DC (1989) The Influence of Formation Properties on the Response of Water Levels in Wells to Earth Tides and Atmospheric Loading. J Geophys Res 14.B9:403-412.

Smith JO (2007) Mathematics of the Discrete Fourier Transform (DFT) with Audio Applications. 2nd ed., Online Book, http://ccrma.stanford.edu/~jos/mdft/.

Sorensen JPR, Butcher AS (2011) Water Level Monitoring Pressure Transducers—A Need for Industry-Wide Standards. Groundwater Monitoring & Remediation, 31: 56–62. doi: 10.1111/j.1745-6592.2011.01346.x

Thomson TW (Lord Kelvin) (1882) On the thermodynamic acceleration of the Earth's rotation. Proc R Soc Edinburgh Session 1881-82 11:396-404

TSoft (2013), A software package for the analysis of Time Series and Earth Tides, http://seismologie.oma.be/TSOFT/tsoft.html (Accessed 15 Jan, 2014)

Van de Kamp G, Gale JE (1983) Theory of earth tides and barometric effects in porous formations with compressible grains. Water Resour Res 19:538-544.

Volland H (1996) Atmosphere and earth's rotation. Surv Geophys 17.1:101-144

Wahr J (1995) "Earth Tides", Global Earth Physics, A handbook of physical constants. AGU Reference Shelf 1, pp 40-46.

Weeks EP (1979) Barometric Fluctuations in Wells Tapping Deep Unconfined Aquifers. Water Resour Res 15.5:1167-1176.

White WN (1932) A method of estimating ground-water supplies based on discharge by plants and evaporation from soil: Results of investigations in Escalante Valley, Utah. Water Supply Paper 659-A, US Geological Survey.

List of Figures

1. Location of the Maules Creek Catchment in New South Wales, Australia.

2. Cross section for Elfin Crossing boreholes.

3. Illustration of the Discrete Fourier Transform (DFT) using simple sine waves: a) 1 cycle per day (cpd) and b) the DFT of a; c) 2 cpd and, d) the DFD of c; e) 0.2 cpd,and f) the DFD of e; f) the summation of these three components (1 cpd, 2 cpd and 0.2 cpd), and h) the resulting DFD.

4. The atmospheric record for the Barologger in BH 8 showing the DFT pairs: a) pressure and temperature, and b) the DFT of the atmospheric pressure. The temperature record from the barlogger (red line) is included in part a) to demonstrate that there is no temperature dependence on the pressure record.

5. DFT pairs for atmospheric pressure observed at BH 8 and the Elfin Crossing surface water level gauge. The complete spectrum is shown in the frequency amplitude plot. a) Time series of barometric pressure; b) DFT of a; c) time series of Elfin Crossing, and d) DFT of c.

6. DFT pairs for piezometer BH 7.1, installed at 10 m depth on the north-west bank of Elfin Crossing (see Fig. 2 for location); a) Time series of barometric pressure and b) is the DFT of a; c) time series of BH 7.1 total pressure and d) is the DFT of c; e) the time series of BH7.1 water levels and f) is the DFT of e.

7. DFT pairs for piezometer EC 17, installed at 5.5 m depth on the opposite bank beneath tree cover (see Fig. 2 for location); a) Time series of barometric pressure and b) is the DFT of a; c) time series of EC 17 total pressure and d) is the DFT of c; e) the time series of EC 17 water levels and f) is the DFT of e.

8. DFT pairs for BH 12.2, installed at 30 m depth close to piezometer 7.1 (see Fig. 2 for location); a) Time series of barometric pressure and b) is the DFT of a; c) time series of BH 12.2 total pressure and d) is the DFT of c; e) the time series of BH 12.2 water levels and f) is the DFT of e. The Earth tide frequencies are identified in the DFT plot.

9. Comparison of a) corrected hydraulic heads and b) atmospheric pressure, for BH 7.1 and BH 12.2. Note the inverted phase of the atmospheric pressure signal in BH 12.2 data and also the completely different phase and frequencies of the unconfined signal of BH 7.1.

10. Envelopes of the seasonal variation of the K_1, M_2 and S_2 components of the hydraulic head at BH 12.2.

11. Composite data for BH 9 at installed at 12.7 m depth (close to EC 17) showing water level change, solar radiation and potential evaporation.

12. Plots showing the amplitude vs time of the 1 cpd signal in EC17, BH 7.1 and the creek.

13. Time series data for the 1 cpd and 2 cpd components of the atmospheric pressure and the BH 12.2 hydraulic head data: a) data for the total series for S_1 and K_1 frequencies showing atmosphere in magenta and BH 12.2 in green; b) expanded to show the phase and amplitude relationships; c) data for the S_2 frequencies; d) expanded to show the phase and amplitude relationships.

14. Barometric efficiency calculation: The spectrum of the calculated earth tide is shown in red and scaled on the left-hand axis. The measured spectrum of the BH 12.2 response is shown in blue and scaled on the right-hand axis.

15.

Table 1. Construction and logger details for the piezometers used in this study (locations are shown in Fig. 2). All unvented loggers were manufactured by Solinst for a range of 20 m (1.5 m for the baro logger).

Name	**Elevation to top of casing (m AHD)**	**Screen length (m)**	**Elevation of mid-point of screen (m AHD)**	**Logger ID**
BH 7.1	258.721	0.15	248.026	2004775 Edge
BH 7.2	258.721	1.5	242.241	1058991 Gold
BH 8 (baro logger)	258.382	1.5	253.587	1044805 Gold
BH 9	254.275	1.0	241.640	1044960 Gold
BH 12.2	259.164	0.15	229.389	2003344 Edge
EC17	255.67	0.15	250.180	1057878 Gold

Table 2. Principal solar and lunar earth tide components.

Symbol	**Frequency (cpd)**	**Period (hours)**	**Vertical amplitude (mm)**	**Explanation**
O_1	0.92953	25.819	158.11	Main lunar diurnal
K_1	1.00273	23.934	191.78	Lunar-solar diurnal
M_2	1.93227	12.421	384.83	Main lunar semi-diurnal
S_2	2.00000	12.000	179.05	Main solar semidiurnal
N_2	1.89598	12.658	73.69	Lunar elliptic (lunar semi-diurnal)

Table 3. Amplitude and probable cause of the observed spectra at 1.00, 1.93 and 2.00 cpd frequencies.

Location	**Tide component (cpd)**	**Amplitude (mm)**	**Probable Cause**
Bore 8 (baro logger)	1.0	7.10	S_{1a}
	2.0	8.15	S_{2a}
BH 7.1	1.0	0.57	Evapotranspiration
BH 12.2	0.93	0.55	Earth tide O_1
	1.0	0.68	S_{1a} mixed with earth tide K_1
	1.90	0.26	Earth tide N_2
	1.93	1.16	Earth tide M_2
	2.0	1.13	S_{2a} mixed with earth tide S_2
EC17	1.0	1.15	Evapotranspiration
	2.0	0.3	Evapotranspiration
Stream	1.0	0.55	Evapotranspiration

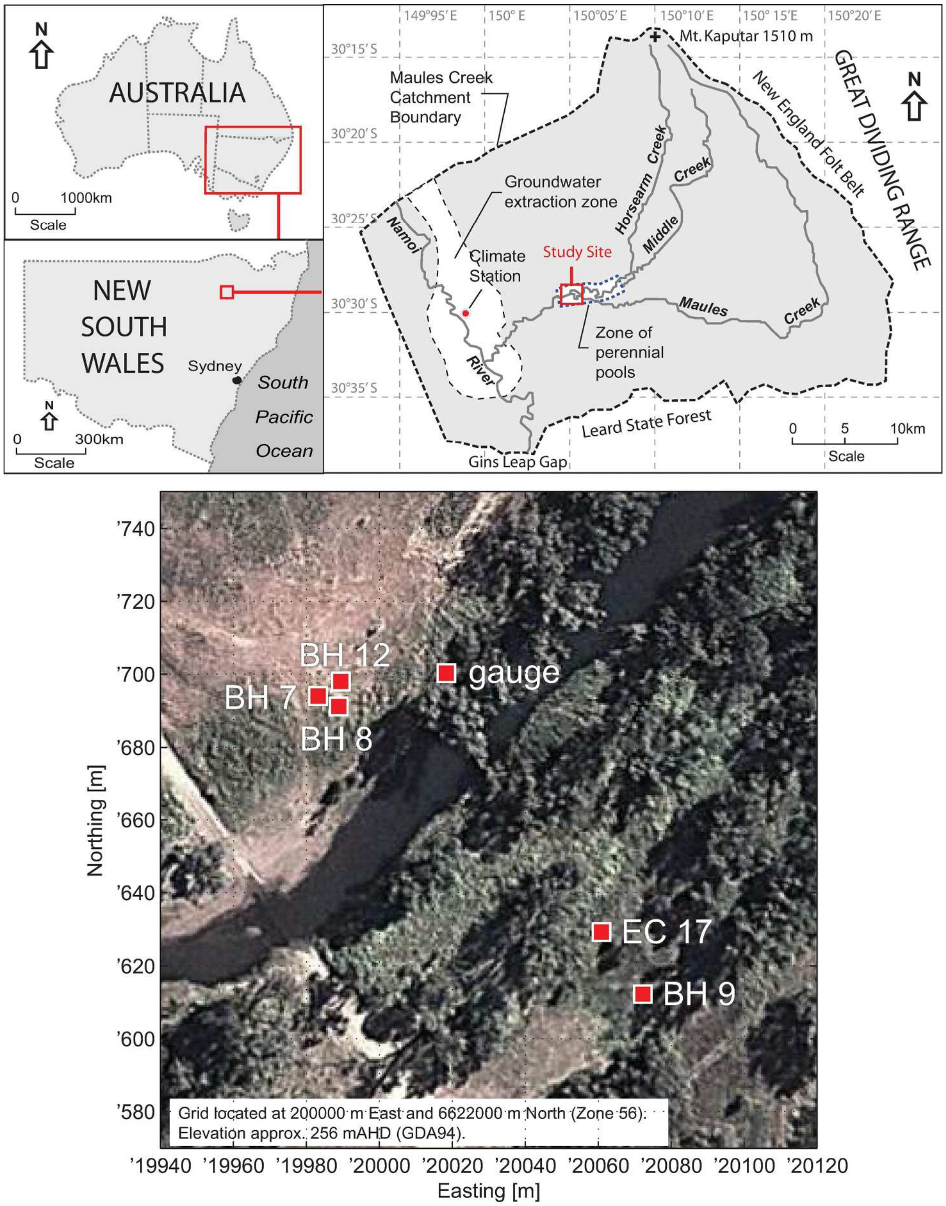

1. Location of the Maules Creek Catchment in New South Wales, Australia.
204x261mm (300 x 300 DPI)

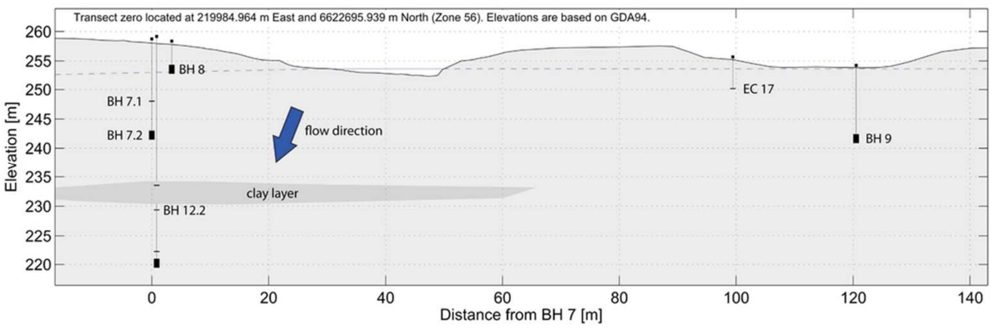

2. Cross section for Elfin Crossing boreholes.
87x29mm (300 x 300 DPI)

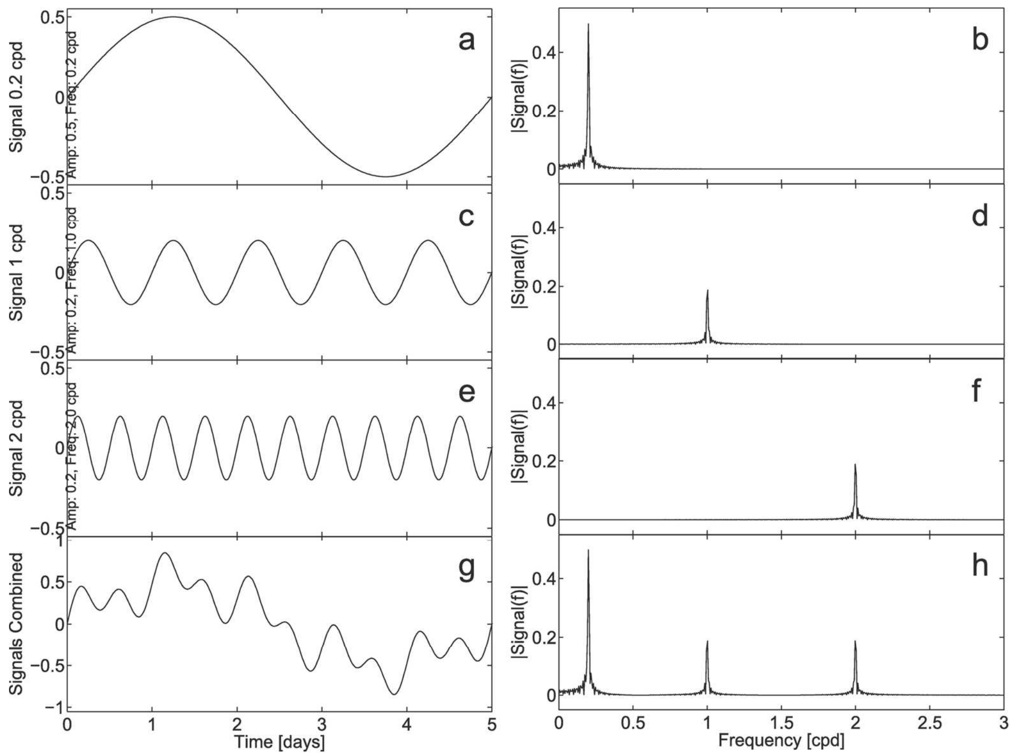

3. Illustration of the Discrete Fourier Transform (DFT) using simple sine waves: a) 1 cycle per day (cpd) and b) the DFT of a; c) 2 cpd and, d) the DFD of c; e) 0.2 cpd,and f) the DFD of e; f) the summation of these three components (1 cpd, 2 cpd and 0.2 cpd), and h) the resulting DFD.
149x111mm (300 x 300 DPI)

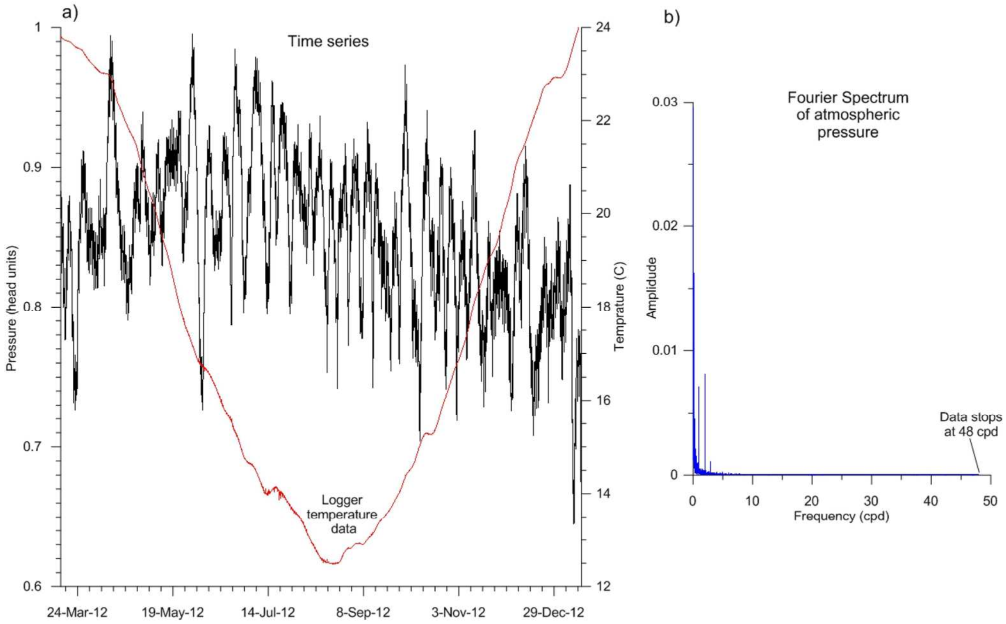

4. The atmospheric record for the Barologger in BH 8 showing the DFT pairs: a) pressure and temperature, and b) the DFT of the atmospheric pressure. The temperature record from the barlogger (red line) is included in part a) to demonstrate that there is no temperature dependence on the pressure record.
165x102mm (300 x 300 DPI)

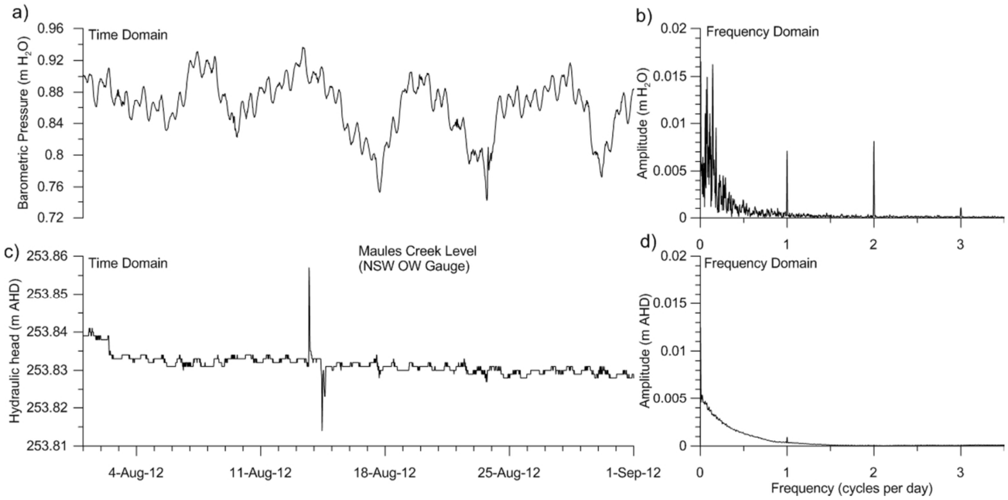

5. DFT pairs for atmospheric pressure observed at BH 8 and the Elfin Crossing surface water level gauge. The complete spectrum is shown in the frequency amplitude plot. a) Time series of barometric pressure; b) DFT of a; c) time series of Elfin Crossing, and d) DFT of c.
130x64mm (300 x 300 DPI)

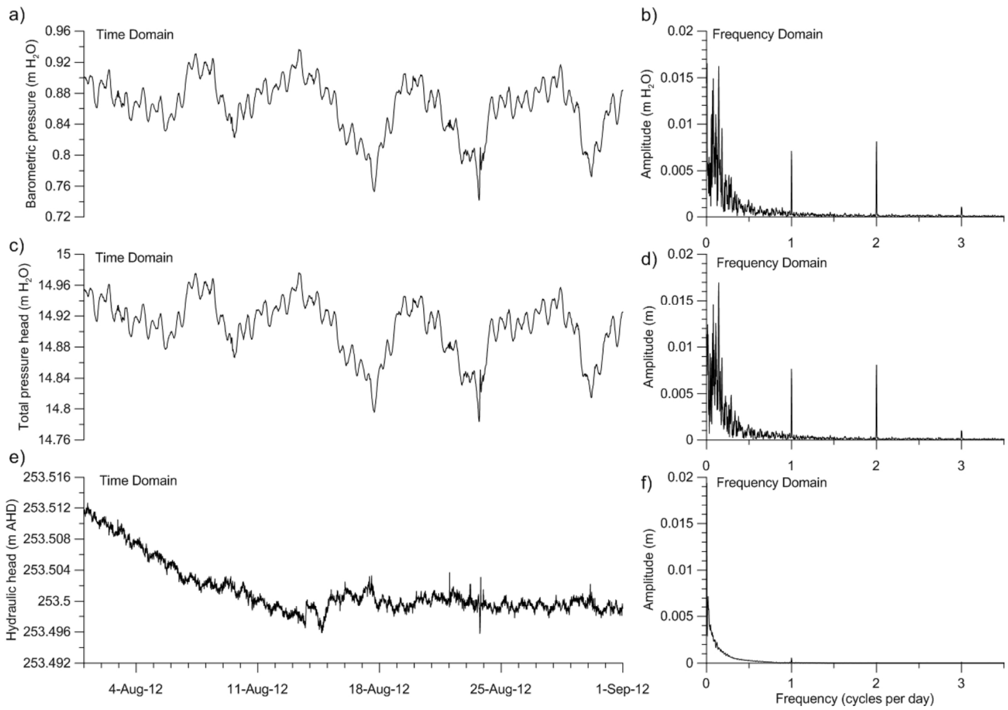

6. DFT pairs for piezometer BH 7.1, installed at 10 m depth on the north-west bank of Elfin Crossing (see Fig. 2 for location); a) Time series of barometric pressure and b) is the DFT of a; c) time series of BH 7.1 total pressure and d) is the DFT of c; e) the time series of BH7.1 water levels and f) is the DFT of e.
188x132mm (300 x 300 DPI)

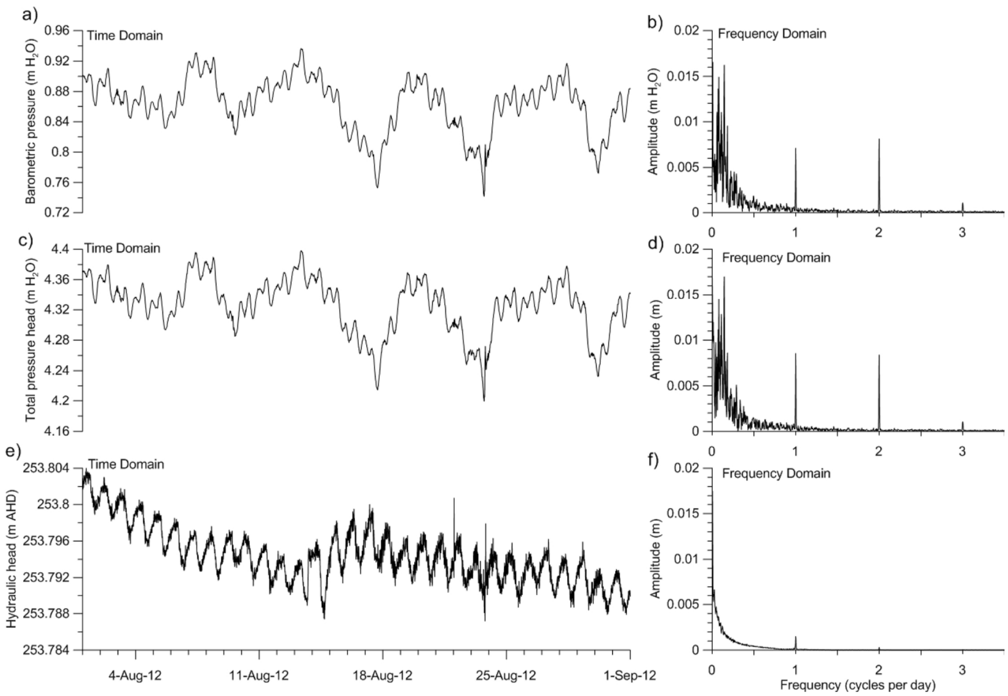

7. DFT pairs for piezometer EC 17, installed at 5.5 m depth on the opposite bank beneath tree cover (see Fig. 2 for location); a) Time series of barometric pressure and b) is the DFT of a; c) time series of EC 17 total pressure and d) is the DFT of c; e) the time series of EC 17 water levels and f) is the DFT of e.
188x130mm (300 x 300 DPI)

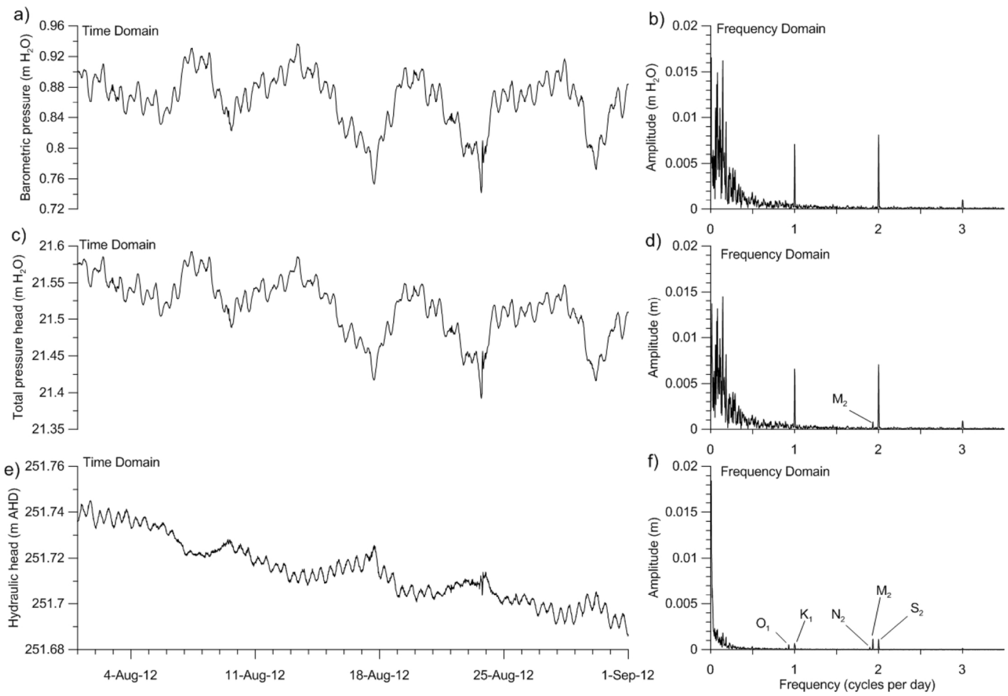

8. DFT pairs for BH 12.2, installed at 30 m depth close to piezometer 7.1 (see Fig. 2 for location); a) Time series of barometric pressure and b) is the DFT of a; c) time series of BH 12.2 total pressure and d) is the DFT of c; e) the time series of BH 12.2 water levels and f) is the DFT of e. The Earth tide frequencies are identified in the DFT plot.
187x129mm (300 x 300 DPI)

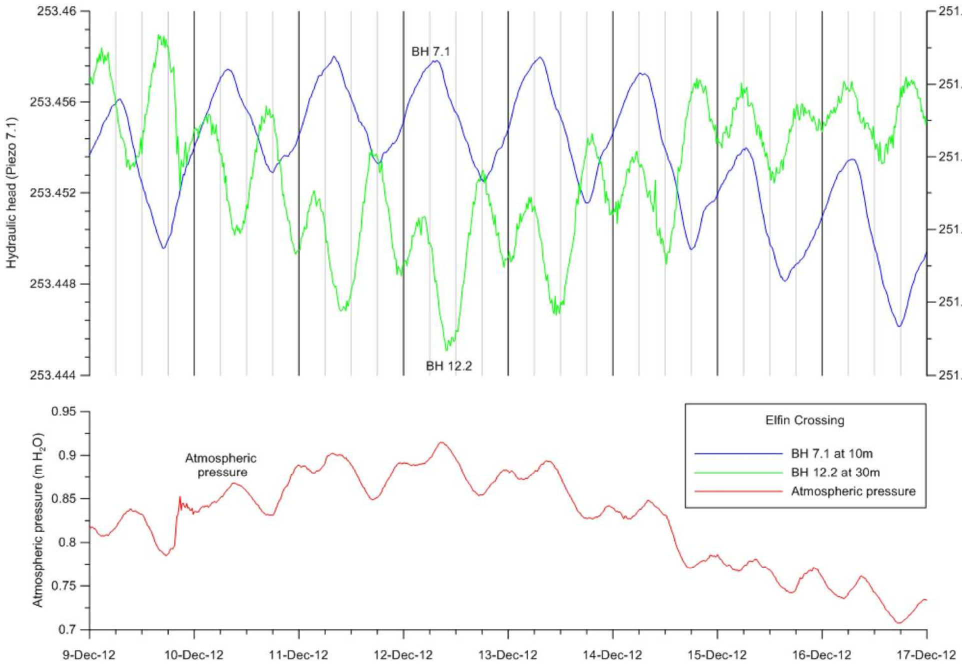

9. Comparison of atmospheric pressure and corrected hydraulic heads for BH 7.1 and BH 12.2. Note the inverted phase of the atmospheric pressure signal in BH 12.2 data and also the completely different phase and frequencies of the unconfined signal of BH 7.1.
180x119mm (300 x 300 DPI)

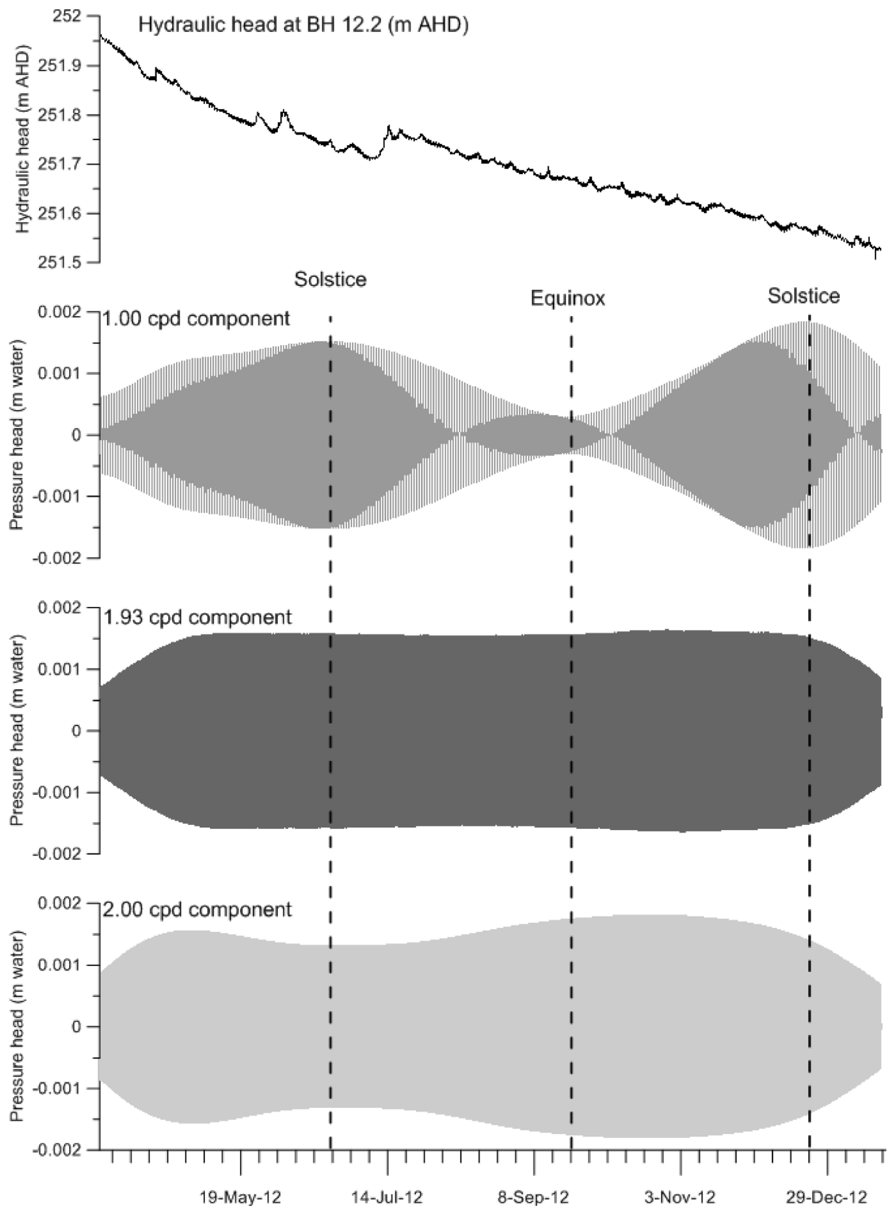

10. Envelopes of the seasonal variation of the K1, M2 and S2 components of the hydraulic head at BH 12.2.
243x331mm (300 x 300 DPI)

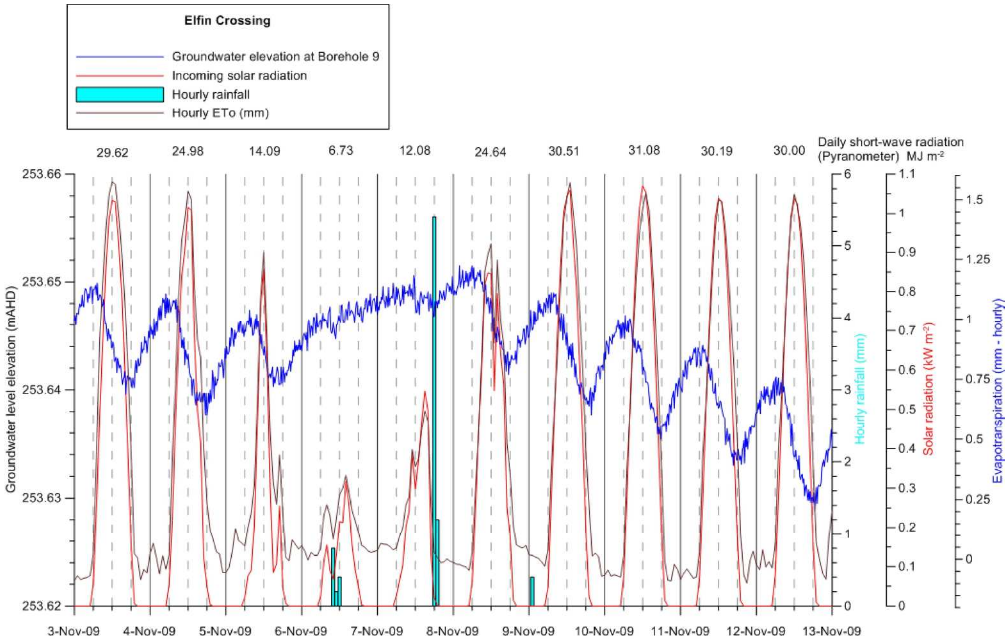

11. Composite data for BH 9 at installed at 12.7 m depth (close to EC 17) showing water level change, solar radiation and potential evaporation.
175x111mm (300 x 300 DPI)

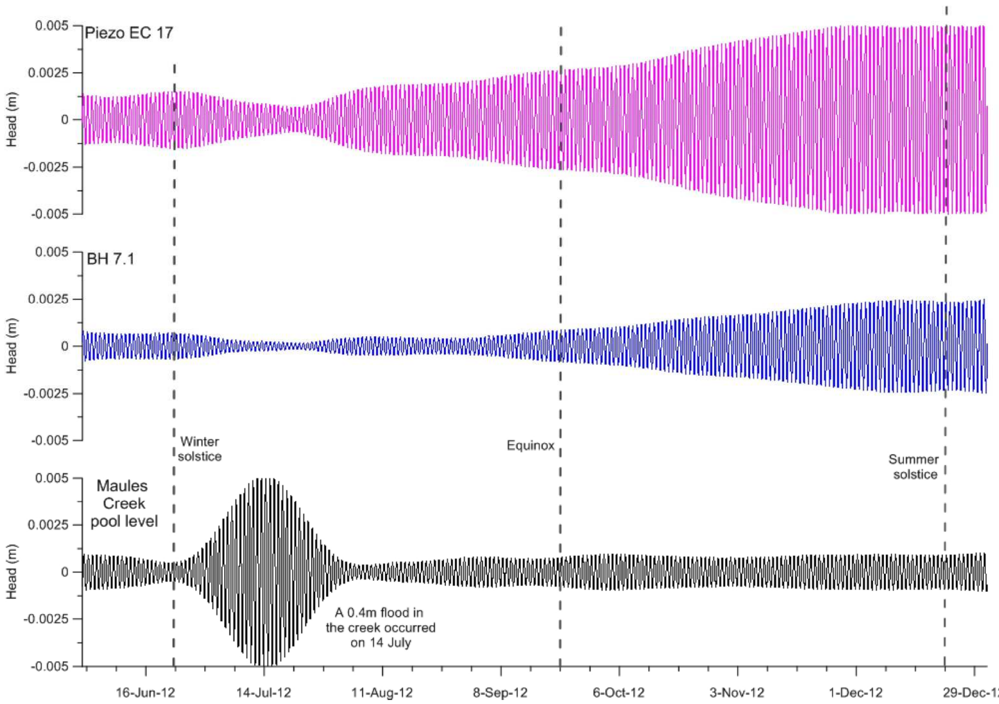

12. Plots showing the amplitude vs time of the 1 cpd signal in EC17, BH 7.1 and the creek.
184x127mm (300 x 300 DPI)

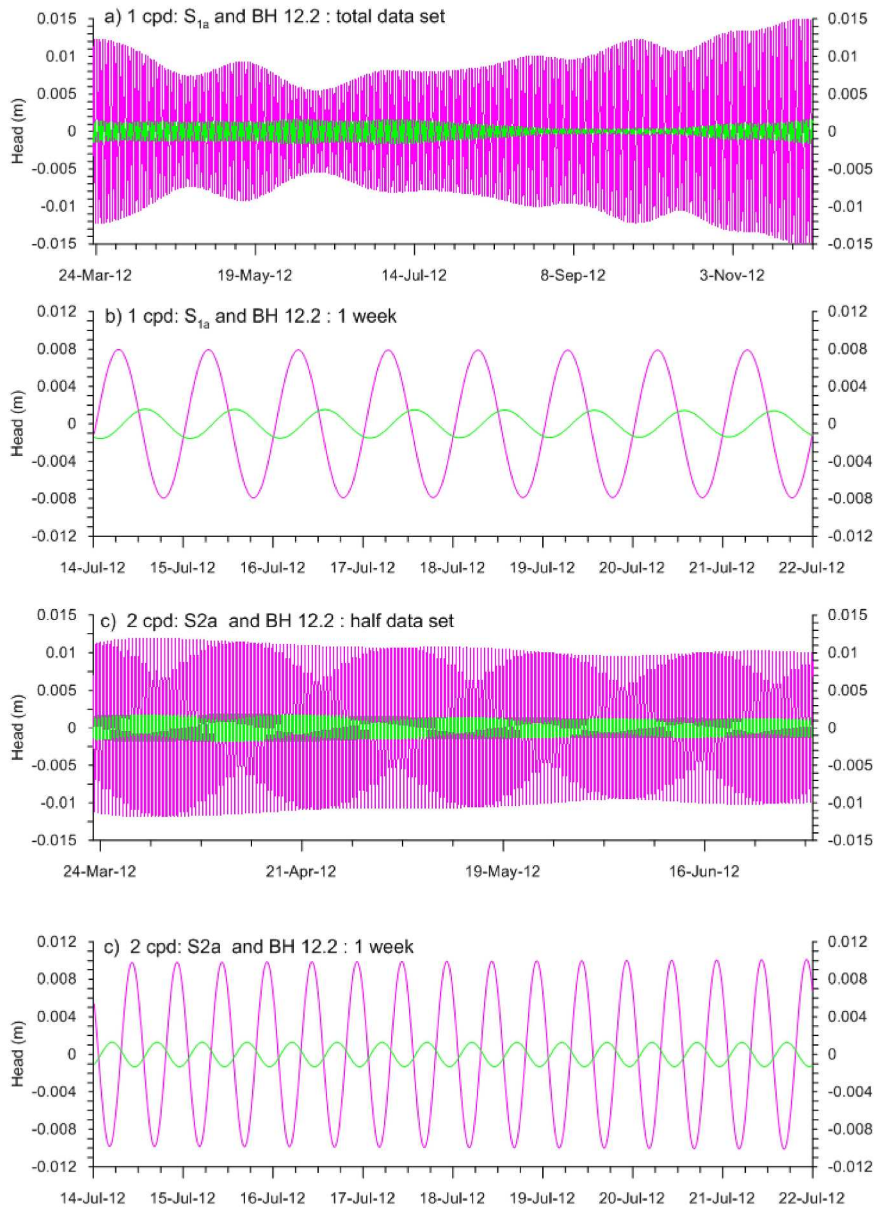

13. Time series data for the 1 cpd and 2 cpd components of the atmospheric pressure and the BH 12.2 hydraulic head data: a) data for the total series for S1 and K1 frequencies showing atmosphere in magenta and BH 12.2 in green; b) expanded to show the phase and amplitude relationships; c) data for the S2 frequencies; d) expanded to show the phase and amplitude relationships.
266x369mm (300 x 300 DPI)

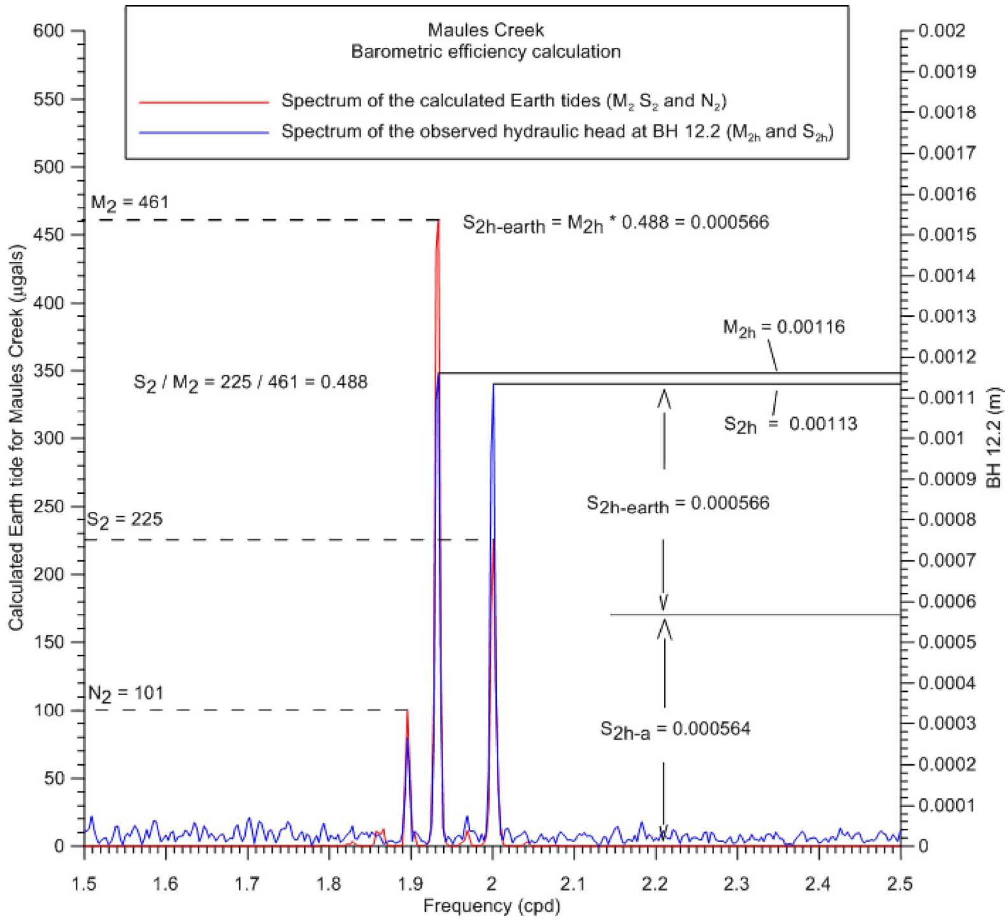

14. Barometric efficiency calculation: The spectrum of the calculated earth tide is shown in red and scaled on the left-hand axis. The measured spectrum of the BH 12.2 response is shown in blue and scaled on the right-hand axis.
170x154mm (300 x 300 DPI)